Transport Coefficients of Oligo- and Poly(α-methylstyrene)s in Dilute Solution

Ikuko Suda, Yumiko Tominaga, Masashi Osa,† Takenao Yoshizaki, and Hiromi Yamakawa*

Department of Polymer Chemistry, Kyoto University, Kyoto 606-8501, Japan

Received July 5, 2000; Revised Manuscript Received September 25, 2000

ABSTRACT: The intrinsic viscosity [η] was determined for 25 samples of atactic oligo- and poly(α-methylstyrene)s (a-PαMS), each with the fraction of racemic diads $f_r = 0.72$, in the range of weight-average molecular weight M_w from 2.94×10^2 (dimer) to 3.22×10^6 in cyclohexane at 30.5 °C (Θ). The translational diffusion coefficient D was also determined from dynamic light-scattering measurements for 21 of them in the range of M_w from 5.30×10^2 (tetramer) to 3.22×10^6 under the same solvent condition. It is found that the double-logarithmic plots of [η] and M_wD against M_w follow their respective asymptotic straight lines of slope $^1/_2$ for $M_w \gtrsim 2 \times 10^5$, but deviate upward and downward, respectively, from them with decreasing M_w for smaller M_w. From an analysis of these transport coefficients on the basis of the helical wormlike (HW) chain model, it is shown that the above M_w dependence of [η] and D may be well explained by the corresponding HW theories with the values of the model parameters consistent with those previously determined from the mean-square radius of gyration $\langle S^2 \rangle$. A comparison is also made of the present results for [η] and D for a-PαMS with the previous ones for atactic polystyrene with $f_r = 0.59$, atactic poly(methyl methacrylate) (a-PMMA) with $f_r = 0.79$, and isotactic PMMA with $f_r \simeq 0.01$. It confirms the previous conclusion derived from $\langle S^2 \rangle$ concerning the chain stiffness and local chain conformations of the a-PαMS chain. That is, the a-PαMS chain tends to retain large and clearly distinguishable helical portions in dilute solution just as the a-PMMA chain, although the strength of helical nature is somewhat smaller for the former.

Introduction

In the preceding paper,[1] the second paper of this series on experimental studies of dilute solution properties of atactic oligo- and poly(α-methylstyrene)s (a-PαMS) with the fraction of racemic diads $f_r = 0.72$ on the basis of the helical wormlike (HW) chain model,[2,3] we have reported results for the scattering function P_s determined in the unperturbed state (in cyclohexane at Θ). It has been found that they may be well explained by the corresponding HW chain theory using the values of the model parameters determined in a first paper[4] from an analysis of the mean-square radius of gyration $\langle S^2 \rangle$ under the same solvent condition. It has then been confirmed that the a-PαMS chain is of rather strong helical nature like the atactic poly(methyl methacrylate) (a-PMMA) chain with $f_r = 0.79$,[2,5] although its strength is smaller for the former. It may therefore be expected that such a character of the a-PαMS chain is also reflected in the behavior of steady-state transport coefficients such as the intrinsic viscosity [η] and translational diffusion coefficient D. Thus, in the present study, we further determine them from viscosity and dynamic light scattering (DLS) measurements for a-PαMS (in cyclohexane at Θ) and compare the results with the HW theories and also with the previous experimental results obtained for atactic polystyrene (a-PS) with $f_r = 0.59$,[6,7] a-PMMA with $f_r = 0.79$,[8,9] and isotactic (i-) PMMA with $f_r \simeq 0.01$.[10]

For a-PMMA[8,9] (with a strong helical nature), the double-logarithmic plot of [η] against the weight-average molecular weight M_w deviates appreciably upward from its asymptotic straight line of slope $^1/_2$ with decreasing M_w for $M_w \lesssim 6 \times 10^4$, following an inverse S-shaped curve, while the same plot of M_wD against M_w deviates downward from its asymptotic straight line of slope $^1/_2$ with decreasing M_w for $M_w \lesssim 5 \times 10^4$, following an S-shaped curve. On the other hand, for a-PS[6,7] and i-PMMA[10] (both with a weak helical nature), both plots follow their respective asymptotic straight lines down to the range of rather small M_w ($\simeq 5 \times 10^3$). Considering the strength of helical nature of the a-PαMS chain mentioned above, the behavior of its [η] and D may be expected to be similar to that for a-PMMA.[8,9] The main purpose of this paper is to confirm this expectation experimentally and examine whether such behavior may be well explained by the HW theories.

As was pointed out in the first paper,[4] the Θ temperature 30.5 °C determined there for our a-PαMS samples in cyclohexane is somewhat lower than literature values.[11−14] If the Θ temperature were incorrect, neither [η] nor M_wD would be proportional to $M_w^{1/2}$ even in the range of very large M_w ($\gtrsim 10^5$) because of the excluded-volume effect. Therefore, the confirmation of the asymptotic behavior of [η] and D is another purpose of this paper.

Experimental Section

Materials. Most of the a-PαMS samples used in this work are the same as those used in the previous studies[1,4] of $\langle S^2 \rangle$ and $P_s(k)$, i.e., fractions separated by preparative gel permeation chromatography (GPC) or fractional precipitation from the original samples prepared by living anionic polymerization.[15] We note that the sample AMS40 is a fraction from the commercial sample 20538-2 from Polymer Laboratories Ltd. We also used additional samples OAMS2, OAMS3, and OAMS4 separated by preparative GPC from the same original sample as that of the samples OAMS5−OAMS13. The samples OAMS2 and OAMS3 were confirmed by ^{1}H and ^{13}C NMR to be completely monodisperse, and the sample OAMS4, by

† Research Fellow of the Japan Society for the Promotion of Science.

10.1021/ma001155u CCC: $19.00
Published on Web 11/16/2000

Table 1. Values of M_w, x_w, M_w/M_n, and f_r for Atactic Oligo- and Poly(α-methylstyrene)s

sample	M_w	x_w	M_w/M_n	f_r
OAMS2[a]	2.94×10^2	2	1	0.56
OAMS3	4.12×10^2	3	1	0.73
OAMS4	5.30×10^2	4	<1.01	
OAMS5	6.48×10^2	5	<1.01	
OAMS6	7.66×10^2	6	<1.01	
OAMS7	8.84×10^2	7	<1.01	
OAMS8[b]	1.04×10^3	8.29	1.01	
OAMS10	1.27×10^3	10.3	1.01	
OAMS13	1.60×10^3	13.1	1.02	0.71
OAMS19	2.27×10^3	18.7	1.07	0.72
OAMS25	2.96×10^3	24.6	1.06	0.72
OAMS33	3.95×10^3	33.0	1.04	0.72
OAMS38	4.57×10^3	38.2	1.07	0.72
OAMS67	7.97×10^3	67.1	1.04	0.72
AMS1	1.30×10^4	109	1.02	0.73
AMS2	2.48×10^4	209	1.02	0.73
AMS5	5.22×10^4	442	1.02	0.73
AMS6	6.46×10^4	547	1.03	0.72
AMS11	1.15×10^5	973	1.04	0.73
AMS15	1.46×10^5	1240	1.02	0.73
AMS24	2.38×10^5	2010	1.05	0.73
AMS40	4.07×10^5	3450	1.02	0.73
AMS80	8.50×10^5	7200	1.05	0.72
AMS200	2.06×10^6	17400	1.05	0.72
AMS320	3.22×10^6	27300		0.73

[a] M_ws of OAMS2 through OAMS7 had been determined by ^{1}H and ^{13}C NMR and GPC. [b] M_ws of OAMS8 through AMS320 had been determined from LS in cyclohexane at 30.5 °C.

analytical GPC to be almost monodisperse.[15] We note that the initiating chain end of each polymerized sample is a *sec*-butyl group and the other end is a hydrogen atom.

The values of M_w determined from ^{1}H and ^{13}C NMR spectra, by analytical GPC, or from (static) light scattering (LS) measurements (in cyclohexane at 30.5 °C), the weight-average degree of polymerization x_w estimated from M_w, f_r determined from ^{1}H and ^{13}C NMR spectra, and the ratio of M_w to the number-average molecular weight M_n determined by analytical GPC are given in Table 1. Although f_r of the samples OAMS4−OAMS10 could not be determined because of the complexity of their ^{1}H NMR spectra, they may be regarded as having almost the same value of f_r as OAMS3 or OAMS13 ($0.71 \lesssim f_r \lesssim 0.73$), since the nine samples OAMS2−OAMS13 are fractions from one original sample.[15] As seen from the values of f_r, all the samples except OAMS2 have the fixed stereochemical composition $f_r = 0.72 \pm 0.01$. The difference in f_r between the sample OAMS2 and the others may be regarded as arising from that in reaction mechanism; i.e., f_r of the former is determined by the termination reaction with methanol, while those of the latter are determined (mainly) by the propagation reaction. As seen from the values of M_w/M_n, all the samples except AMS320 are very narrow in molecular weight distribution. Although the value of M_w/M_n for the sample AMS320 could not be determined with high accuracy because of the lack of the GPC calibration curve in the necessary range, its molecular weight distribution may be considered to be as narrow as that of the other samples.

The solvent cyclohexane used for viscosity and DLS measurements was purified according to a standard procedure.

Viscosity. Viscosity measurements were carried out for all the samples listed in Table 1 in cyclohexane at 30.5 °C (Θ). For the measurements, we used conventional capillary and four-bulb spiral capillary viscometers of the Ubbelohde type. The flow time was measured to a precision of 0.1 s, keeping the difference between those of the solvent and solution larger than 20 s. The test solutions were maintained at a constant temperature within ±0.005 °C during the measurements.

The test solutions were prepared by continuous stirring at 50 °C for 3−7 days. The polymer mass concentrations c (in g/cm^3) were calculated from the weight fractions with the densities of the solutions. The density of each solution was calculated with the partial specific volume v_2 of the polymer and the density ρ_0 of the solvent. The quantities v_2 and ρ_0 were measured with a pycnometer of the Lipkin−Davison type having the volume of 10 cm^{-3}. Density corrections were also made in the calculations of the relative viscosity η_r from the flow times of the solution and solvent. The data obtained for the specific viscosity η_{sp} and η_r were treated as usual by the Huggins and Fuoss−Mead plots, respectively, to determine $[\eta]$ and the Huggins coefficient k'.

Dynamic Light Scattering. DLS measurements were carried out to determine D for all the samples except OAMS2, OAMS3, OAMS5, and OAMS7 in cyclohexane at 30.5 °C (Θ) by the use of a Brookhaven Instruments model BI-200SM light scattering goniometer with vertically polarized incident light of wavelength $\lambda_0 = 488$ nm from a Spectra-Physics model 2020 argon ion laser equipped with a model 583 temperature-stabilized etalon for a single-frequency-mode operation. The photomultiplier tube used was EMI 9863B/350, the output from which was processed by a Brookhaven Instruments model BI-9000AT Digital Correlator. (An electric shutter was attached to the original detector alignment in order to monitor the dark count automatically.) The normalized autocorrelation function $g^{(2)}(t)$ of scattered light intensity $I(t)$ at time t was measured at four or five concentrations and at scattering angles θ ranging from 18 to 105°. The most concentrated solution of each sample was prepared in the same manner as in the case of the viscosity measurements. It was optically purified by filtration through a Teflon membrane of pore size 0.45 or 0.10 μm. The solutions of lower concentrations were obtained by successive dilution. The polymer mass concentrations c were calculated from the weight fractions with the densities of the solutions.

From the data for $g^{(2)}(t)$ so determined at finite concentrations c, we determine D at an infinitely long time at infinite dilution in the same manner as that used in the previous studies.[7,16] At small c, the plot of $(^1/_2)\ln[g^{(2)}(t) - 1]$ against t in general follows a straight line represented by

$$(^1/_2)\ln[g^{(2)}(t) - 1] = \text{const} - At \tag{1}$$

with A the slope for such large t that all the internal motions of solute polymer chains have relaxed away.

With the slope A evaluated from the plot, we may determine the apparent diffusion coefficient $D^{(LS)}(c)$ at finite c from

$$D^{(LS)}(c) = \lim_{k \to 0} A/k^2 \tag{2}$$

where k is the scattering vector and is given by

$$k = (4\pi/\tilde{\lambda})\sin(\theta/2) \tag{3}$$

with $\tilde{\lambda}$ the wavelength of the incident light in the solvent. At very small c, $D^{(LS)}(c)$ may be expanded as

$$D^{(LS)}(c) = D^{(LS)}(0)(1 + k_D^{(LS)}c + ...) \tag{4}$$

so that the desired $D = D(\infty)$ (at an infinitely long time) may be determined by an extrapolation of $D^{(LS)}(c)$ to $c = 0$ as

$$D = D^{(LS)}(0) \tag{5}$$

The values of the refractive index n_0 at $\lambda_0 = 488$ nm and of the viscosity coefficient η_0 for cyclohexane at 30.5 °C are 1.425_6 and 0.818 cP, respectively. The former value was estimated by a linear interpolation of the plot of n_0 against λ_0^{-2} with the values 1.429_8 and 1.422_3 of n_0 at $\lambda_0 = 436$ and 546 nm, respectively. We note that the values 1.429_8 and 1.422_3 of n_0 at 30.5 °C were calculated from an interpolation formula[17] as a function of temperature.

Results

Intrinsic Viscosity [η]. Intrinsic viscosity data for all the a-PαMS samples in cyclohexane at 30.5 °C (Θ) are summarized in Table 2 along with the values of the

Table 2. Results of Viscometry for Atactic Oligo- and Poly(α-methylstyrene)s in Cyclohexane at 30.5 °C

sample	$[\eta]$, dL/g	k'
OAMS2	0.0159	0.86
OAMS3	0.0250	0.85
OAMS4	0.0292	0.79
OAMS5	0.0319	0.88
OAMS6	0.0346	0.82
OAMS7	0.0363	0.82
OAMS8	0.0379	0.79
OAMS10	0.0420	0.81
OAMS13	0.0453	0.81
OAMS19	0.0512	0.71
OAMS25	0.0552	0.73
OAMS33	0.0615	0.75
OAMS38	0.0644	0.71
OAMS67	0.0794	0.78
AMS1	0.0972	0.69
AMS2	0.126	0.63
AMS5	0.176	0.63
AMS6	0.193	0.65
AMS11	0.247	0.67
AMS15	0.284	0.64
AMS24	0.344	0.73
AMS40	0.435	0.69
AMS80	0.645	0.68
AMS200	0.993	0.68
AMS320	1.22	0.63

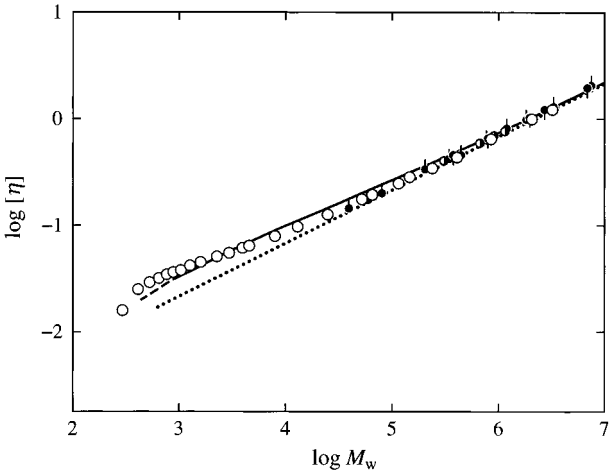

Figure 1. Double-logarithmic plots of $[\eta]$ (in dL/g) against M_w for a-PαMS in cyclohexane at 30.5 °C: (○) present data; (filled circles with pip up) data by Noda et al. (obtained at 34.5 °C);[18] (filled circles with pip down) data by Tsunashima (obtained at 34.9 °C);[13] (◑) data by Hadjichristidis et al. (obtained at 36.0 °C).[19] The solid curve represents the best-fit HW theoretical values for $N \geq 2$, the dashed line segment connecting the values for $N = 1$ and 2. The dotted straight line has a slope of $^1/_2$.

Huggins coefficient k'. It is seen from the table that k' decreases with increasing M_w as in the case of a-PS[6] in cyclohexane at 34.5 °C (Θ) but does not exhibit a minimum such as observed for a- and i-PMMAs[8,10] in acetonitrile at 44.0 and 28.0 °C (Θ), respectively.

In Figure 1, the present data (unfilled circles) for $[\eta]$ (in dL/g) for a-PαMS in cyclohexane at 30.5 °C (Θ) are double-logarithmically plotted against M_w. In the figure the dotted line represents the asymptotic straight line of slope $^1/_2$. The data points follow this straight line for $M_w \gtrsim 2 \times 10^5$, confirming that the Θ temperature is 30.5 °C for a-PαMS with $f_r = 0.72$ in cyclohexane. For $M_w \lesssim 2 \times 10^5$, they deviate definitely upward from the asymptotic straight line and form an inverse S-shaped curve as a whole. As mentioned in the Introduction, such behavior of the plot is characteristic of a polymer chain of strong helical nature such as a-PMMA. We note that such characteristic behavior would remain unchanged if the true Θ temperature were somewhat higher than 30.5 °C. In the figure the solid curve and the dashed line segment represent the best-fit HW theoretical values, which are discussed in the next (Discussion) section.

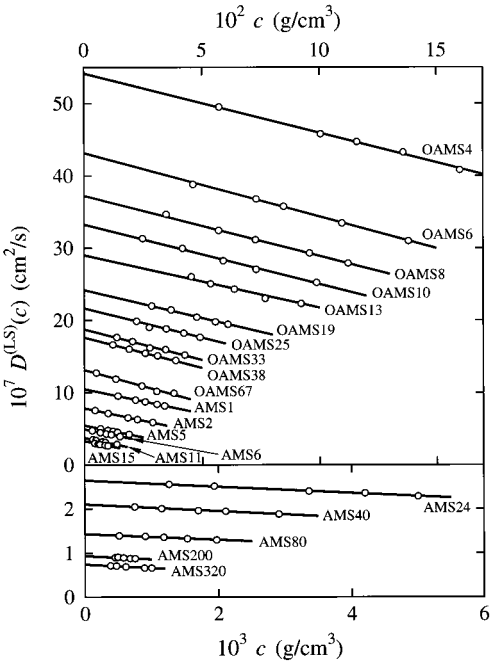

Figure 2. Plots of $D^{(LS)}(c)$ against c for the indicated a-PαMS samples in cyclohexane at 30.5 °C.

For comparison, literature data for a-PαMS in cyclohexane are also plotted in the figure for the samples with $f_r \simeq 0.63$ at 34.5 °C by Noda et al.[18] (filled circles with pip up), those with $f_r \simeq 0.68$ at 34.9 °C by Tsunashima[13] (filled circles with pip down), and those with $f_r \simeq 0.74$ at 36.0 °C by Hadjichristidis et al.[19] (right-half-filled circles). It is seen that all the literature data are in rather good agreement with ours (within ca. 5%). This is inconsistent with the fact that the values of $\langle S^2 \rangle$ obtained by Kato et al.[20] for the same samples Noda et al.[18] used (for $[\eta]$) and also those by Li et al.[21] for the same samples Hadjichristidis et al.[19] used (for $[\eta]$) are appreciably larger (>13 %) than ours (see Figure 5 of ref 4).

Translational Diffusion Coefficient *D*. The data points for $(^1/_2)$ ln$[g^{(2)}(t) - 1]$ as a function of t directly obtained from the DLS measurements for each test solution at each scattering angle θ were found to follow a straight line, so that the slope A could be unambiguously determined. Further, in the range of k (or θ) where the DLS measurements were carried out, the ratio A/k^2 was independent of k within experimental error for all the test solutions, although we do not show the results. Then $D^{(LS)}(c)$ for each solution was determined as a mean of the observed values of A/k^2 over k. $D^{(LS)}(c)$ so obtained are plotted against c in Figure 2 for the 21 indicated samples in cyclohexane at 30.5 °C (Θ). The data points for each sample are seen to follow a straight line, and therefore $D^{(LS)}(0)$ $(=D)$ and $k_D^{(LS)}$ in eq 4 may be accurately determined from its ordinate intercept and slope, respectively. The values of D and $k_D^{(LS)}$ so obtained for a-PαMS in cyclohexane at 30.5 °C are given in Table 3. For convenience, in its last column

Table 3. Results of DLS Measurements for Atactic Oligo- and Poly(α-methylstyrene)s in Cyclohexane at 30.5 °C

sample	10^7D, cm²/s	$k_D^{(LS)}$, cm³/g	R_H, Å
OAMS4	54.2	−1.5	5.02
OAMS6	43.2	−2.0	6.29
OAMS8	37.2	−2.2	7.35
OAMS10	33.3	−2.5	8.16
OAMS13	29.0	−2.5	9.38
OAMS19	24.2	−3.2	11.2
OAMS25	21.7	−3.8	12.5
OAMS33	18.8	−4.5	14.5
OAMS38	17.6	−4.8	15.5
OAMS67	13.2	−6.9	20.6
AMS1	10.5	−6.5	25.9
AMS2	7.85	−8.8	34.6
AMS5	5.47	−12	49.7
AMS6	4.94	−13	55.0
AMS11	3.74	−18	72.7
AMS15	3.30	−20	82.4
AMS24	2.65	−27	103
AMS40	2.10	−36	129
AMS80	1.43	−45	190
AMS200	0.932	−78	292
AMS320	0.739	−110	368

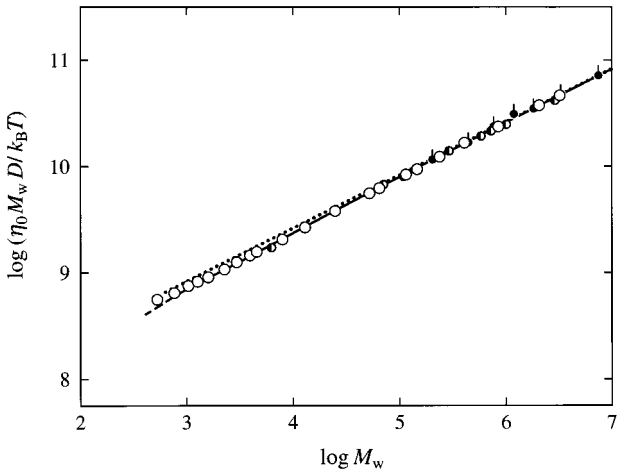

Figure 3. Double-logarithmic plots of $\eta_0 M_w D/k_B T$ (in cm^{-1}) against M_w for a-PαMS in cyclohexane at 30.5 °C: (○) present data; (filled circles with pip up) data by Noda et al. (obtained at 34.5 °C);[22] (◐) data by Cotts and Selser (obtained at 35.0 °C).[23] The solid curve represents the best-fit HW theoretical values for $N \geq 2$, with the dashed line segment connecting the values for $N = 1$ and 2. The dotted straight line has a slope of $^1/_2$.

there are also given the values of the hydrodynamic radius R_H calculated from the defining equation

$$R_H = k_B T/6\pi\eta_0 D \tag{6}$$

where k_B is the Boltzmann constant, T is the absolute temperature, and η_0 is the viscosity coefficient of the solvent. The values of $k_D^{(LS)}$ are negative for all the samples as in the cases of a-PS[7] and a- and i-PMMAs[9,10] under their respective Θ conditions.

In Figure 3, $\eta_0 M_w D/k_B T$ (in cm^{-1}) calculated from the present data for D for a-PαMS in cyclohexane at 30.5 °C (Θ) are double-logarithmically plotted against M_w (unfilled circles). In the figure the dotted line represents the asymptotic straight line of slope $^1/_2$. The data points follow this straight line for $M_w \gtrsim 2 \times 10^5$ as in the case of $[\eta]$, reconfirming the correctness of the Θ temperature 30.5 °C for the present system. In contrast to the case of $[\eta]$, they deviate downward from the asymptotic straight line for $M_w \lesssim 2 \times 10^5$ and form an S-shaped curve as a whole, although the deviation is not so appreciable as that in the case of $[\eta]$. In the figure the solid curve and the dashed line segment represent the best-fit HW theoretical values, which are discussed in the next (Discussion) section.

For comparison, literature data for a-PαMS in cyclohexane are also plotted in the figure for the samples with $f_r \simeq 0.63$ at 34.5 °C by Noda et al.[22] (filled circles with pip up) and those with $f_r \simeq 0.74$ at 35.0 °C by Cotts and Selser[23] (left-half-filled circles). We note that Noda et al.[22] reported the values of the sedimentation coefficient s for the same samples Kato et al.[20] used (for $\langle S^2 \rangle$) and Noda et al.[18] also used (for $[\eta]$ above), and therefore we have converted their values of s to the above corresponding values of D by the use of the relation

$$D = N_A k_B T s/M_w(1 - v_2\rho_0) \tag{7}$$

with N_A the Avogadro constant. The data by Noda et al.[22] are in rather good agreement with ours (within ca. 5%), while the results for $\langle S^2 \rangle$ for the same samples[20] are appreciably larger than ours, as mentioned above. The data by Cotts and Selser are also in good agreement with ours.

Discussion

Analysis of $[\eta]$ on the Basis of the HW Model. We first analyze the data for $[\eta]$ on the basis of the HW touched-bead model.[2,24] The HW chain itself[2,3] may be described in terms of four basic model parameters: the differential-geometrical curvature κ_0 and torsion τ_0 of its characteristic helix taken at the minimum zero of its elastic energy, the static stiffness parameter λ^{-1}, and the shift factor M_L defined as the molecular weight per unit contour length. For the touched-bead model chain of total contour length $L = Nd_b$ with N the number of beads in the chain and d_b the diameter of the bead, $[\eta]$ may be written in the form[2,24]

$$[\eta] = (1/\lambda^2 M_L) f_\eta(\lambda L; \lambda^{-1}\kappa_0, \lambda^{-1}\tau_0, \lambda d_b) \tag{8}$$

where the function f_η is defined by

$$f_\eta(\lambda L) = \lambda^{-1} M_L[\bar{\eta}] \tag{9}$$

with $[\bar{\eta}]$ being the $[\eta]$ measured in units of $(\lambda^{-1})^3$ and being given by eq 6.111 with eqs 6.113 and 6.120 of ref 2. It satisfies the following asymptotic relation

$$\lim_{\lambda L \to \infty} [f_\eta(\lambda L)/(\lambda L)^{1/2}] = c_\infty^{3/2} \Phi_\infty \tag{10}$$

where c_∞ is given by

$$c_\infty = \frac{4 + (\lambda^{-1}\tau_0)^2}{4 + (\lambda^{-1}\kappa_0)^2 + (\lambda^{-1}\tau_0)^2} \tag{11}$$

and Φ_∞ denotes the (theoretical) coil-limiting value 2.87 $\times 10^{23}$ mol^{-1} of the Flory−Fox factor $\Phi = M[\eta]/(6\langle S^2 \rangle)^{3/2}$ with M the molecular weight (for the unperturbed chain in the limit of $\lambda L \to \infty$). We note that the above theoretical result for $[\eta]$ does not depend on the sign of τ_0, i.e., the handiness of helices, and this is the case with D. We also note that Φ is the reduced hydrodynamic volume[2] defined as the ratio of the hydrodynamic

Table 4. Values of the HW model Parameters for Atactic Poly(α-methylstyrene) in Cyclohexane at 30.5 °C

$\lambda^{-1}\kappa_0$	$\lambda^{-1}\tau_0$	λ^{-1}, Å	M_L, Å^{-1}	d_b, Å	obsd quantity
3.0	1.2	43.0	42.3	10.3	$[\eta]$
(3.0)	(1.2)	56.2	38.0	10.7	D
3.0	0.9	46.8	39.8		$\langle S^2\rangle$[a]

[a] See ref 4.

(molar) volume V_H to $\langle S^2\rangle^{3/2}$

$$\Phi = V_H/\langle S^2\rangle^{3/2} \tag{12}$$

with

$$V_H = 6^{-3/2}M[\eta] \tag{13}$$

The basic equations required for an analysis of the data may then be written as

$$\log[\eta] = \log f_\eta(\lambda L) - \log(\lambda^2 M_L) \tag{14}$$

$$\log M_w = \log(\lambda L) + \log(\lambda^{-1}M_L) \tag{15}$$

Thus, the quantities $\lambda^2 M_L$ and $\lambda^{-1}M_L$ (and therefore λ^{-1} and M_L) may be estimated from a best fit of double-logarithmic plots of the theoretical f_η against λL for properly chosen values of $\lambda^{-1}\kappa_0$, $\lambda^{-1}\tau_0$, and λd_b to that of the observed $[\eta]$ against M_w, so that we may determine $\lambda^{-1}\kappa_0$, $\lambda^{-1}\tau_0$, λ^{-1}, M_L, and d_b as usual (as mentioned in Chapter 6 of ref 2).

In Figure 1, the solid curve associated with the present data points (unfilled circles) represents the best-fit theoretical values calculated from eq 8 with $\lambda^{-1}\kappa_0 = 3.0$, $\lambda^{-1}\tau_0 = 1.2$, $\lambda d_b = 0.24$, $\log(\lambda^2 M_L) = -1.64$, and $\log(\lambda^{-1}M_L) = 3.26$ for $N \geq 2$, the dashed line segment connecting those values for $N = 1$ and 2. As in the case of a-PMMA[8] with a strong helical nature, the theoretical curve reproduces semiquantitatively the inverse S-shaped one experimentally observed, although agreement between them is somewhat better in the present case of a-PαMS. The values of the HW model parameters so determined are listed in the first row of Table 4. In the third row there are also given the values of the model parameters (except d_b) determined in the first paper[4] from $\langle S^2\rangle$. The value of $\lambda^{-1}\tau_0$ determined from $[\eta]$ is somewhat larger than that from $\langle S^2\rangle$, but this does not change the previous conclusion[1,4] concerning the helical nature of the a-PαMS chain. With the values of the model parameters $\lambda^{-1}\kappa_0$, $\lambda^{-1}\tau_0$, and λ^{-1} determined from $[\eta]$, the radius ρ [$=\kappa_0/(\kappa_0^2 + \tau_0^2)$] and pitch h [$=2\pi\tau_0/(\kappa_0^2 + \tau_0^2)$] of the characteristic helix are calculated to be 12.4 Å and 31.1 Å, respectively, which are in good agreement with 14.3 Å and 27.0 Å, respectively, determined from $\langle S^2\rangle$.[4] The values of λ^{-1} and M_L determined from $[\eta]$ are somewhat different from the corresponding ones determined from $\langle S^2\rangle$. This may be regarded as arising from the disagreement between the theoretical and experimental values of Φ_∞, as often mentioned.[2,16] However, the differences are not so large as those in the cases of a- and i-PMMAs,[2] since the observed value of Φ_∞ for a-PαMS shown later is closer to the above theoretical value than those for the PMMAs. Thus the two sets of parameter values from the two different properties may rather be considered to be consistent with each other.

Analysis of *D* on the Basis of the HW Model. The quantity $\eta_0 M_w D/k_B T$ for the same HW touched-bead model as above may be written in the form[2,7]

$$\eta_0 M_w D/k_B T = (M_L/3\pi)f_D(\lambda L; \lambda^{-1}\kappa_0, \lambda^{-1}\tau_0, \lambda d_b) \tag{16}$$

where the function f_D is given by eq 6.64 of ref 2 and may be evaluated numerically by the use of the interpolation formula given by eq 6.28 of ref 2 for the mean reciprocal end-to-end distance of the chain. The function f_D satisfies the following asymptotic relation

$$\lim_{\lambda L\to\infty}[f_D(\lambda L)/(\lambda L)^{1/2}] = (\sqrt{6}/2)c_\infty^{-1/2}\rho_\infty \tag{17}$$

where c_∞ is given by eq 11 and ρ_∞ denotes the (Kirkwood theoretical) coil-limiting value 1.505 of the ratio ρ of $\langle S^2\rangle^{1/2}$ to R_H (for the unperturbed chain in the limit of $\lambda L \to \infty$).[2] We note that ρ^{-1} is the reduced hydrodynamic radius[2] defined as the ratio of R_H to $\langle S^2\rangle^{1/2}$

$$\rho^{-1} = R_H/\langle S^2\rangle^{1/2} \tag{18}$$

The basic equations required for an analysis of the data may then be written as

$$\log(\eta_0 M_w D/k_B T) = \log f_D(\lambda L) + \log M_L - 0.975 \tag{19}$$

along with eq 15. Thus, in this case, the quantities M_L and $\lambda^{-1}M_L$ may be estimated from a best fit of double-logarithmic plots of the theoretical f_D against λL for properly chosen values of $\lambda^{-1}\kappa_0$, $\lambda^{-1}\tau_0$, and λd_b to that of the observed $\eta_0 M_w D/k_B T$ against M_w, so that we may in principle determine the five parameters $\lambda^{-1}\kappa_0$, $\lambda^{-1}\tau_0$, λ^{-1}, M_L, and d_b. In the case of D, however, all these five parameters are difficult to determine by the curve fitting as above, since the experimental double-logarithmic plot of $\eta_0 M_w D/k_B T$ against M_w does not appreciably deviate from its asymptotic straight line of slope $^1/_2$, as seen from Figure 3. For simplicity, therefore, we assume that the values of $\lambda^{-1}\kappa_0$ and $\lambda^{-1}\tau_0$ are the same as those determined above from $[\eta]$, and we determine the remaining three parameters λ^{-1}, M_L, and d_b.

In Figure 3, the solid curve associated with the present data points (unfilled circles) represents the best-fit theoretical values calculated from eq 16 with $\lambda d_b = 0.19$, $\log M_L = 1.58$, and $\log(\lambda^{-1} M_L) = 3.33$ for $N \geq 2$, the dashed line segment connecting those values for $N = 1$ and 2. Agreement between theory and experiment is seen to be very good. The values of the HW model parameters so determined are listed in the second row of Table 4. With these parameter values, the radius ρ and pitch h are calculated to be 16.1 Å and 40.6 Å, respectively. The value 56.2 Å of λ^{-1} determined from D is definitely larger than those determined from $\langle S^2\rangle$ and $[\eta]$, while the value of M_L determined from D is somewhat smaller than those determined from $\langle S^2\rangle$ and $[\eta]$. This tendency is the same as that in the cases of a-PS and a- and i-PMMAs previously[2] studied (see Tables 5.1 and 6.3 of ref 2). As often mentioned,[2,16] it may be regarded as arising from the disagreement between the theoretical and experimental values of Φ_∞ (mentioned above) and ρ_∞. Note that their theoretical values have been obtained for Gaussian chains without consideration of the fluctuation in hydrodynamic interaction.[2] As for d_b, the values from $[\eta]$ and D are in rather good agreement with each other in this case, and are slightly larger than those for a-PS (see Table 6.3 of ref 2). Considering these facts, it may be concluded that

Table 5. Values of Φ_∞(cord) and ρ_∞(cord)

polymer (f_r)	solvent	temp, °C	$10^{-23}\Phi_\infty$(cord), mol^{-1}	ρ_∞(cord)
a-PαMS (0.72)	cyclohexane	30.5	2.79 ± 0.09	1.26 ± 0.02
a-PS (0.59)[a]	cyclohexane	34.5	2.79 ± 0.08	1.26 ± 0.01
a-PMMA (0.79)	acetonitrile	44.0	2.34 ± 0.06	1.29 ± 0.02
i-PMMA (0.01)	acetonitrile	28.0	2.58 ± 0.11	1.25 ± 0.02

[a] The values of Φ_∞(cord) and ρ_∞(cord) for a-PS and a- and i-PMMAs have been reproduced from ref 2.

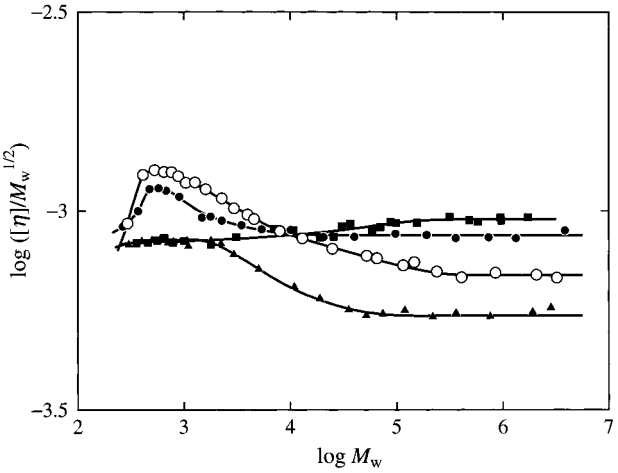

Figure 4. Double-logarithmic plots of $[\eta]/M_w^{1/2}$ (in dL/g) against $M_w = 72$: (○) present data for a-PαMS with $f_r = 0.72$ in cyclohexane at 30.5 °C; (●) previous data for a-PS with $f_r = 0.59$ in cyclohexane at 34.5 °C;[6,16,25] (▲) previous data for a-PMMA with $f_r = 0.79$ in acetonitrile at 44.0 °C;[8,16,27] (■) previous data for i-PMMA with $f_r \simeq 0.01$ in acetonitrile at 28.0 °C.[10,29] The solid curve connects smoothly the data points for each polymer.

the HW theory may rather give a consistent explanation of the results for the three properties $\langle S^2\rangle$, $[\eta]$, and D.

Comparison with the Other Polymers. We make a comparison of the present results for $[\eta]$ and D for the unperturbed a-PαMS chain with those previously obtained for the unperturbed a-PS[6,7,16,25,26] and a- and i-PMMA[8,9,10,16,27−29] chains. For this purpose, $[\eta]/M_w^{1/2}$ (in dL/g) and $\eta_0 M_w^{1/2} D/k_B T$ (in cm^{-1}) (instead of $[\eta]$ and $\eta_0 M_w D/k_B T$ in Figures 1 and 3) are double-logarithmically plotted against M_w in Figures 4 and 5, respectively, for a-PαMS in cyclohexane at 30.5 °C (Θ) (unfilled circles), a-PS in cyclohexane at 34.5 °C (Θ) (filled circles),[6,7,16,25,26] a-PMMA in acetonitrile at 44.0 °C (Θ) (filled triangles),[8,9,16,27,28] and i-PMMA in acetonitrile at 28.0 °C (Θ) (filled squares).[10,28,29] The solid curve connects smoothly the data points for each polymer. It is seen that as M_w is decreased, the two kinds of plots for both a-PαMS and a-PMMA deviate appreciably upward and downward, respectively, from their respective asymptotic values (in the limit of $M_w \to \infty$) for $M_w \lesssim 10^5$, while those for a-PS and i-PMMA are almost independent of M_w for $M_w \gtrsim 10^4$. The results clearly reflect the differences in chain stiffness and local chain conformation between the four polymers, the strength of helical nature being larger for a-PαMS and a-PMMA than for the other two. The values of the model parameters determined from $\langle S^2\rangle$ for a-PS and a- and i-PMMAs are given in Tables 4 and 5 of the first paper.[4]

Finally, we examine the behavior of the reduced hydrodynamic volume Φ and radius ρ^{-1} defined by eqs 12 and 18, respectively, for the four polymers. In Figure 6, the values of Φ (in mol^{-1}) and ρ^{-1} calculated from the observed values of $[\eta]$, D (or R_H), and $\langle S^2\rangle$ are double-

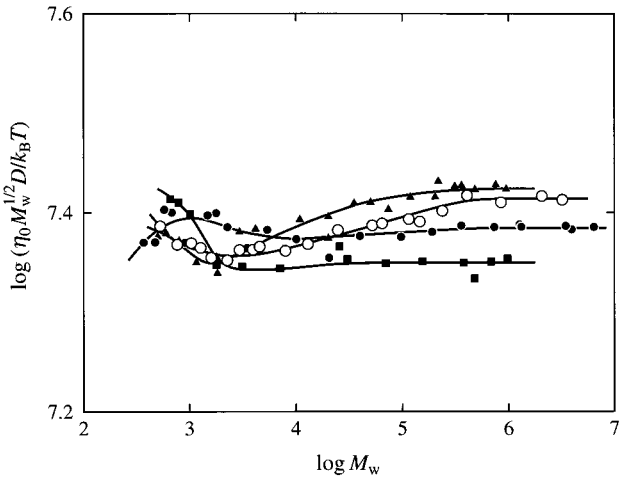

Figure 5. Double-logarithmic plots of $\eta_0 M_w^{1/2} D/k_B T$ (in cm^{-1}) against M_w: (○) present data for a-PαMS with $f_r = 0.72$ in cyclohexane at 30.5 °C; (●) previous data for a-PS with $f_r = 0.59$ in cyclohexane at 34.5 °C;[7,16,26] (▲) previous data for a-PMMA with $f_r = 0.79$ in acetonitrile at 44.0 °C;[9,16,28] (■) previous data for i-PMMA with $f_r \simeq 0.01$ in acetonitrile at 28.0 °C.[10,28] The solid curve connects smoothly the data points for each polymer.

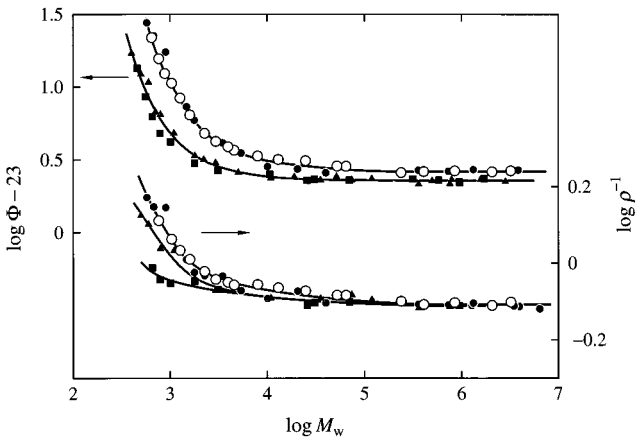

Figure 6. Double-logarithmic plots of Φ (in mol^{-1}) and ρ^{-1} against M_w: (○) present data for a-PαMS with $f_r = 0.72$ in cyclohexane at 30.5 °C; (●) previous data for a-PS with $f_r = 0.59$ in cyclohexane at 34.5 °C;[6,7,16,25,26,30] (▲) previous data for a-PMMA with $f_r = 0.79$ in acetonitrile at 44.0 °C;[5,8,9,16,27,28] (■) previous data for i-PMMA with $f_r \simeq 0.01$ in acetonitrile at 28.0 °C.[10,28,29,31] The solid curves connect smoothly the data points (see the text).

logarithmically plotted against M_w for a-PαMS in cyclohexane at 30.5 °C (Θ) (unfilled circles), a-PS in cyclohexane at 34.5 °C (Θ) (filled circles),[6,7,16,25,26,30] a-PMMA in acetonitrile at 44.0 °C (Θ) (filled triangles),[5,8,9,16,27,28] and i-PMMA in acetonitrile at 28.0 °C (Θ) (filled squares).[10,28,29,31] We note that we have not been able to calculate the values of Φ for the samples OAMS2, OAMS3, OAMS4, AMS11, and AMS15 and those of ρ^{-1} for the samples OAMS4, AMS11, and AMS15, since we did not determine $\langle S^2\rangle$ for these samples in the first paper.[4] It is seen that as M_w is increased, both of the two quantities for the four polymers first decrease for $M_w \lesssim 10^4$, and then become independent of M_w for larger M_w. The plots of Φ for a-PαMS and a-PS are close to each other, and those for a- and i-PMMAs are also close to each other, the latter being definitely lower than the former. The solid curve associated with the data for Φ connects smoothly the data points for each pair. As for ρ^{-1}, the plots for

a-PαMS and a-PS are close to each other as in the case of Φ, while those for PMMAs split into two branches for $M_w \lesssim 5 \times 10^3$. The solid curves associated with the data for ρ^{-1} connect smoothly the data points for the pair of a-PαMS and a-PS and those for a- and i-PMMAs.

The values of Φ_∞ and ρ_∞ for a-PαMS are estimated to be 2.63×10^{23} mol^{-1} and 1.27, respectively, as means of the values for the five samples AMSx with $x = 24$, 40, 80, 200, and 320. For a quantitative comparison of the values of Φ_∞ and ρ_∞, for a-PαMS with those for the other polymers, we make polydispersity corrections to them in the same manner as before, i.e., by the use of the equations[16]

$$\Phi\,(\text{cord}) = [M_z^{3/2}/(M^{1/2})_w M_w]\Phi \tag{20}$$

$$\rho(\text{cord}) = [M_w/(M^{1/2})_w M_z^{1/2}]\rho \tag{21}$$

with M_z and $(M^{1/2})_w$ the z-average molecular weight and the weight average of $M^{1/2}$, respectively. With the values of M_z/M_w and $M_w^{1/2}/(M^{1/2})_w$ determined by analytical GPC for the four samples AMSx with $x = 24$, 40, 80, and 200 (which are not given here), we obtain $(2.79 \pm 0.09) \times 10^{23}$ mol^{-1} and 1.26 ± 0.02 as the corrected values of Φ_∞ and ρ_∞, respectively, for a-PαMS, which are listed in Table 5 along with the corresponding values for a-PS and a- and i-PMMAs reproduced from Table 6.4 of ref 2. The present corrected value of Φ_∞, is almost the same as that for a-PS and is close to the above (Kirkwood) theoretical value 2.87×10^{23} (exactly[2] 2.862×10^{23}). However, the experimental values for them are appreciably larger than those for a- and i-PMMAs, indicating that Φ_∞ cannot be regarded as a universal constant.[2,16] On the other hand, the corrected values of ρ_∞ for the four polymers are not very different but are appreciably smaller than the above Kirkwood value 1.505 (even the Zimm value[2] 1.479). The overestimates of the theoretical Φ_∞ and ρ_∞ arise from the fact that the fluctuation in hydrodynamic interaction has not been considered, as noted above.

Conclusion

We have determined $[\eta]$ and D for a-PαMS with $f_r = 0.72$ in cyclohexane at 30.5 °C (Θ) over a wide range of M_w, including the oligomer region. The double-logarithmic plots of $[\eta]$ and $\eta_0 M_w D/k_B T$ against M_w have been found to follow their respective asymptotic straight lines of slope $^1/_2$ for $M_w \gtrsim 2 \times 10^5$, confirming the correctness of the Θ temperature above for our a-PαMS samples in cyclohexane. As was expected from the strength of helical nature of the a-PαMS chain, the plots of $[\eta]$ and $\eta_0 M_w D/k_B T$ deviate upward and downward, respectively, from their respective asymptotic straight lines with decreasing M_w for $M_w \lesssim 2 \times 10^5$. Such characteristic behavior of the plots may be well explained by the corresponding HW theories by the use of the values of the model parameters consistent with those determined in the first paper[4] from $\langle S^2 \rangle$ and also those used in the preceding paper[1] on P_s, confirming the previous conclusion concerning the chain stiffness and local chain conformations of the a-PαMS chain mentioned in the Introduction.

References and Notes

(1) Ohgaru, Y.; Sumida, M.; Osa, M.; Yoshizaki, T.; Yamakawa, H. *Macromolecules* **2000**, *33*, 9316.
(2) Yamakawa, H. *Helical Wormlike Chains in Polymer Solutions*; Springer: Berlin, 1997.
(3) Yamakawa, H. *Polym. J.* **1999**, *31*, 109.
(4) Osa, M.; Yoshizaki, T.; Yamakawa, H. *Macromolecules* **2000**, *33*, 4828.
(5) Tamai, Y.; Konishi, T.; Einaga, Y.; Fujii, M.; Yamakawa, H. *Macromolecules* **1990**, *23*, 4068 and succeeding papers.
(6) Einaga, Y.; Koyama, H.; Konishi, T.; Yamakawa, H. *Macromolecules* **1989**, *22*, 3419.
(7) Yamada, T.; Yoshizaki, T.; Yamakawa, H. *Macromolecules* **1992**, *25*, 377.
(8) Fujii, Y.; Tamai, Y.; Konishi, T.; Yamakawa, H. *Macromolecules* **1991**, *24*, 1608.
(9) Dehara, K.; Yoshizaki, T.; Yamakawa, H. *Macromolecules* **1993**, *26*, 5137.
(10) Sawatari, N.; Konishi, T.; Yoshizaki, T.; Yamakawa, H. *Macromolecules* **1995**, *28*, 1089.
(11) Cowie, J. M. G.; Bywater, S. *J. Polym. Sci., Part A-2* **1968**, *6*, 499.
(12) Kato, T.; Miyaso, K.; Nagasawa, M. *J. Phys. Chem.* **1968**, *72*, 2161.
(13) Tsunashima, Y. Ph.D. Thesis, Kyoto University, 1972.
(14) Lindner, J. S.; Hadjichristidis, N.; Mays, J. W. *Polym. Commun.* **1989**, *30*, 174.
(15) Osa, M.; Sumida, M.; Yoshizaki, T.; Yamakawa, H.; Ute, K.; Kitayama, T.; Hatada, K. *Polym. J.* **2000**, *32*, 361.
(16) Konishi, T.; Yoshizaki, T.; Yamakawa, H. *Macromolecules* **1991**, *24*, 5614.
(17) Johnson, B. L.; Smith, J. In *Light Scattering from Polymer Solutions*; Huglin, M. B., Ed.; Academic Press: London, 1972; Chapter 2.
(18) Noda, I.; Mizutani, K.; Kato, T.; Fujimoto, T.; Nagasawa, M. *Macromolecules* **1970**, *3*, 787.
(19) Hadjichristidis, N.; Lindner, J. S.; Mays, J. W.; Wilson, W. W. *Macromolecules* **1991**, *24*, 6725.
(20) Kato, T.; Miyaso, K.; Noda, I.; Fujimoto, T.; Nagasawa, M. *Macromolecules* **1970**, *3*, 777.
(21) Li, J.; Harville, S.; Mays, J. W. *Macromolecules* **1997**, *30*, 466.
(22) Noda, I.; Mizutani, K.; Kato, T. *Macromolecules* **1977**, *10*, 618.
(23) Cotts, P. M.; Selser, J. C. *Macromolecules* **1990**, *23*, 2050.
(24) Yoshizaki, T.; Nitta, I.; Yamakawa, H. *Macromolecules* **1988**, *21*, 165.
(25) Abe, F.; Einaga, Y.; Yamakawa, H. *Macromolecules* **1993**, *26*, 1891.
(26) Arai, T.; Abe, F.; Yoshizaki, T.; Einaga, Y.; Yamakawa, H. *Macromolecules* **1995**, *28*, 5458.
(27) Abe, F.; Horita, K.; Einaga, Y.; Yamakawa, H. *Macromolecules* **1994**, *27*, 725.
(28) Arai, T.; Sawatari, N.; Yoshizaki, T.; Einaga, Y.; Yamakawa, H. *Macromolecules* **1996**, *29*, 2309.
(29) Kamijo, M.; Abe, F.; Einaga, Y.; Yamakawa, H. *Macromolecules* **1995**, *28*, 1095.
(30) Konishi, T.; Yoshizaki, T.; Saito, T.; Einaga, Y.; Yamakawa, H. *Macromolecules* **1990**, *23*, 290.
(31) Kamijo, M.; Sawatari, N.; Konishi, T.; Yoshizaki, T.; Yamakawa, H. *Macromolecules* **1994**, *27*, 5697.

MA001155U